Electronic Supplementary Information

Photocatalytic CO_2 reduction on Cu single atoms incorporated in ordered macroporous TiO_2 toward tunable products

Cong Chen [a], Ting Wang [a], Ke Yan [a], Shoujie Liu [b], Yu Zhao [c], Benxia Li [a,*]

[a] *Department of Chemistry, Key Laboratory of Surface & Interface Science of Polymer Materials of Zhejiang Province, Zhejiang Sci-Tech University, Hangzhou 310018, PR China*

[b] *Chemistry and Chemical Engineering of Guangdong Laboratory, Shantou 515063, P. R. China*

[c] *College of Material, Chemistry and Chemical Engineering, Key Laboratory of Organosilicon Chemistry and Material Technology, Ministry of Education, Hangzhou Normal University, Hangzhou, Zhejiang 311121, PR China*

Corresponding Authors. *Email address: libx@zstu.edu.cn (B. X. Li)

1. Supplementary Experiments

1.1. Preparation of polystyrene (PS) colloidal crystal templates

The monodisperse PS submicrospheres are prepared by an emulsifier-free emulsion polymerization method. Specifically, styrene is rinsed by 0.1 M NaOH aqueous solution and deionized water for three times, respectively, to remove the stabilizer. Then, 8.6 mL of the pretreated styrene and 170 mL deionized water are added into a four-neck flask. The mixture is stirred at 400 rpm by an electric blender and heated to 80 ℃ in N_2 atmosphere. When the reaction temperature reaches 80 ℃, 10 mL of 0.1 M $K_2S_2O_8$ aqueous solution is injected into the mixture to trigger the polymerization of styrene. After the polymerization reaction continues for 5 h, the reaction system is cooled to room temperature by ice bath. The PS submicrospheres are collected from the latex and assembled into the PS colloidal crystal templates (CCTs) by centrifugation at 7000 rpm for 0.5 h. Finally, the as-prepared PS CCTs are dried at room temperature for further use.

1.2. Photoelectrochemical tests

The photoelectrochemical tests are conducted in a three-electrode system of an electrochemical workstation (CHI660E, China), with 0.1 M Na_2SO_4 solution as electrolyte. The catalyst-coated fluorine-tin-oxide (FTO) glass, platinum wire and Ag/AgCl electrode are used as photoelectrode, counter electrode, and reference electrode, respectively. For preparing a photoelectrode, 4 mg photocatalyst and 10 μL naphthol are mixed with 390 μL deionized water by sonication to form a slurry, and 200 μL of the slurry was uniformly coated onto a FTO glass (1 cm × 1 cm), which is then dried naturally at room temperature. The transient photocurrent is measured under a chopped light irradiation (light on/off cycles: 30 s) from a 300 W Xe lamp, with a bias potential of 0.11 V. The electrochemical impedance spectra (EIS) are measured in

the frequency range of 0.01-10^5 Hz with an amplitude of 5 mV and a bias potential of 0 V vs. Ag/AgCl electrode. For comparison, the transient photocurrent tests are implemented in the Na_2SO_4 solution electrolyte saturated with Ar and CO_2, respectively.

1.3. Detection of H_2O_2 generated in photocatalytic CO_2 reduction reaction

Hydrogen peroxide (H_2O_2) generated in photocatalytic CO_2 reduction process is determined by an iodimetry method. For the liquid-solid photocatalytic system, 5 mg $Cu_{0.01}$/3DOM-TiO_2 photocatalyst is dispersed in 2 mL CO_2-saturated water. After being exposed to irradiation for 4 h, the suspension is filtered by a syringe filter to remove the catalyst particles for the subsequent detection. For the gas-solid photocatalytic system, 5 mg $Cu_{0.01}$/3DOM-TiO_2 photocatalyst is put in the quartz tube, followed with injecting 0.1 mL H_2O and blowing CO_2 gas into the tube. After 4 h irradiation, 2 mL H_2O is added into the quartz tube to extract H_2O_2 generated during the photocatalytic reaction, and the suspension is then filtered by a syringe filter. 1 mL of the filtrate is added into the mixture of 1 mL potassium hydrogen phthalate ($C_8H_5KO_4$) aqueous solution (0.1 M) and 1 mL potassium iodide (KI) aqueous solution (0.4 M). H_2O_2 can react with I^- ions to produce I^{3-} ions which shows a characteristic absorption at 350 nm. The UV-vis absorption spectra of the testing solutions are recorded in the wavelength range of 300-500 nm on a Shimadzu UV-2600 spectrophotometer. The amount of I_3^- is determined by UV-vis spectroscopy according to its characteristic absorption at 350 nm, and the corresponding amount of H_2O_2 is calculated.

2. Supplementary Figures

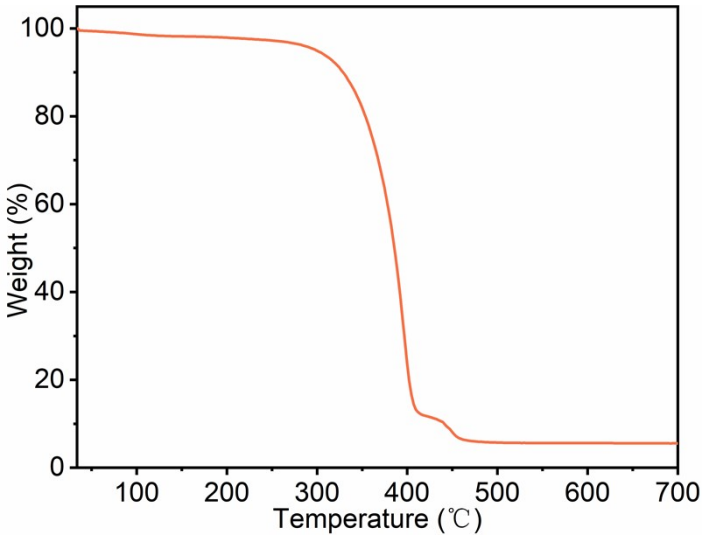

Fig. S1. Thermogravimetric curve of the colloidal crystal templates loaded with precursors.

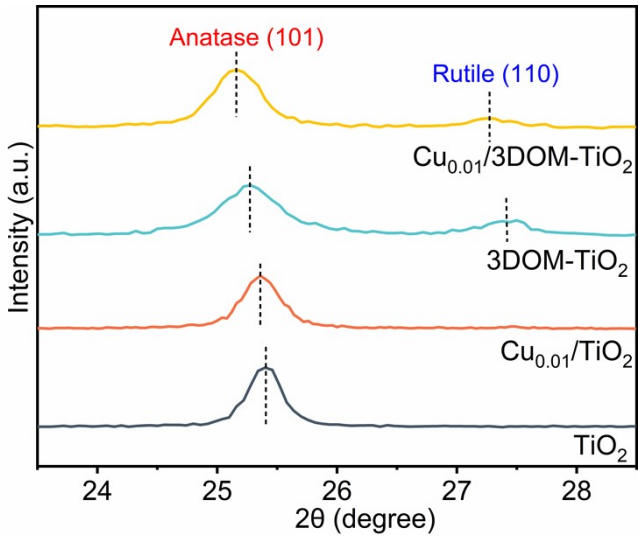

Fig. S2. Locally amplified XRD patterns of different photocatalysts.

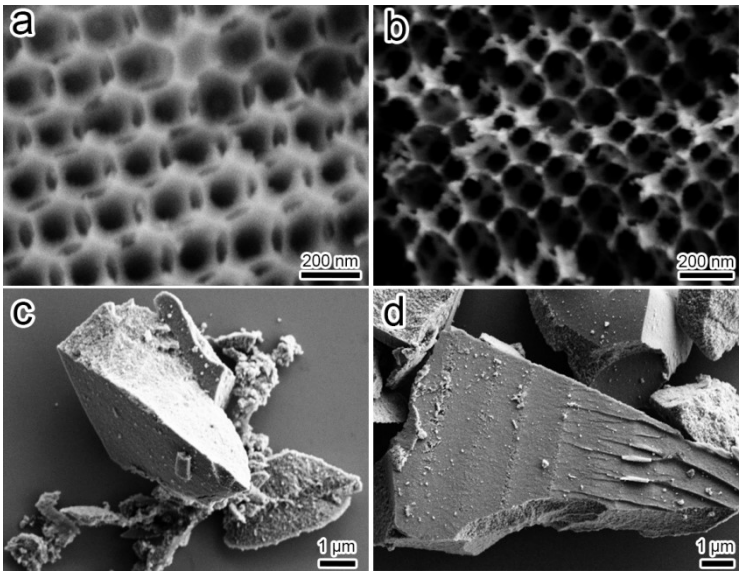

Fig. S3. SEM images of (a) $Cu_{0.01}/3DOM\text{-}TiO_2$, (b) $3DOM\text{-}TiO_2$, (c) $Cu_{0.01}/TiO_2$, (d) TiO_2.

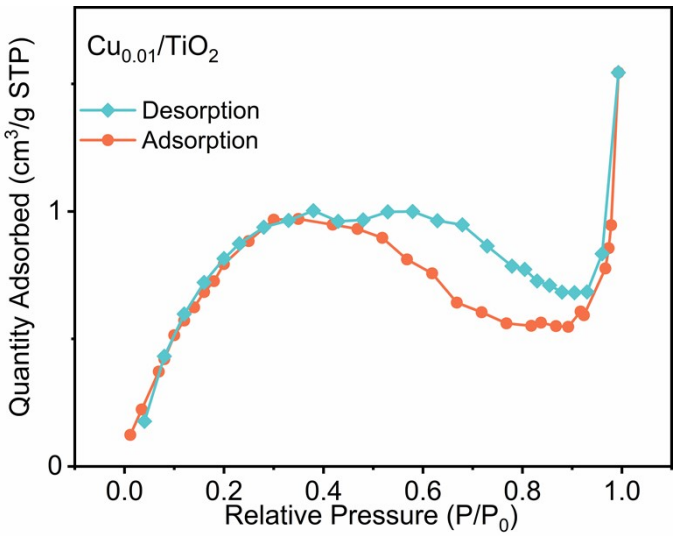

Fig. S4. Nitrogen adsorption-desorption isotherm of $Cu_{0.01}/TiO_2$ sample.

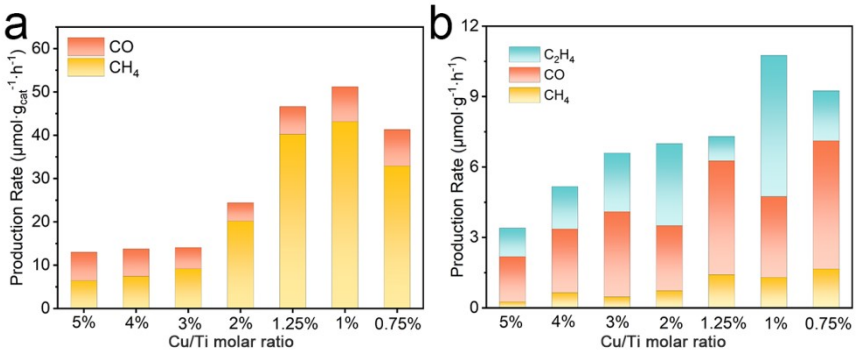

Fig. S5. Photocatalytic CO_2 reduction performance in (a) gas-solid system and (b) liquid-solid system over the $Cu_{0.01}$/3DOM TiO_2 catalysts with different Cu/Ti molar ratios.

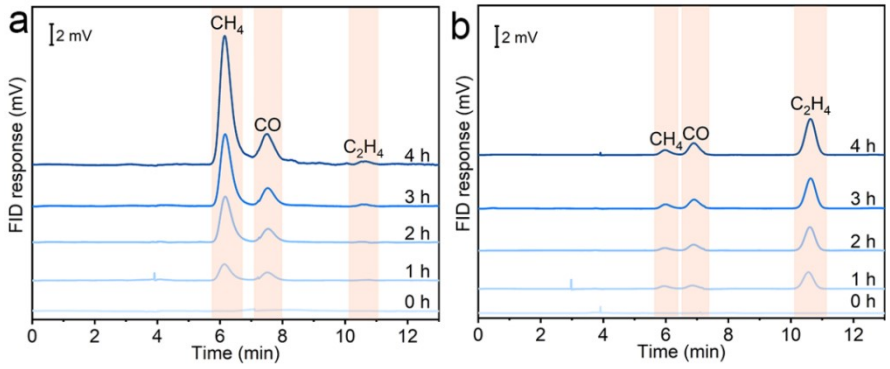

Fig. S6. FID response signals of CH_4, CO and C_2H_4 in the photocatalytic CO_2 reduction reaction with $Cu_{0.01}$/3DOM-TiO_2 catalyst in (a) gas-solid catalytic system and (b) liquid-solid catalytic system.

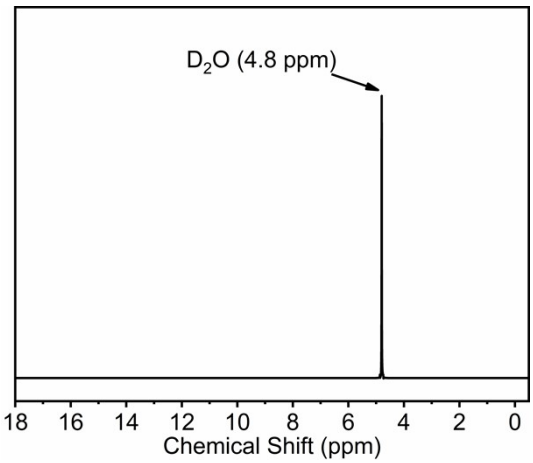

Fig. S7. NMR detection of the photocatalytic CO_2 reduction reaction solution.

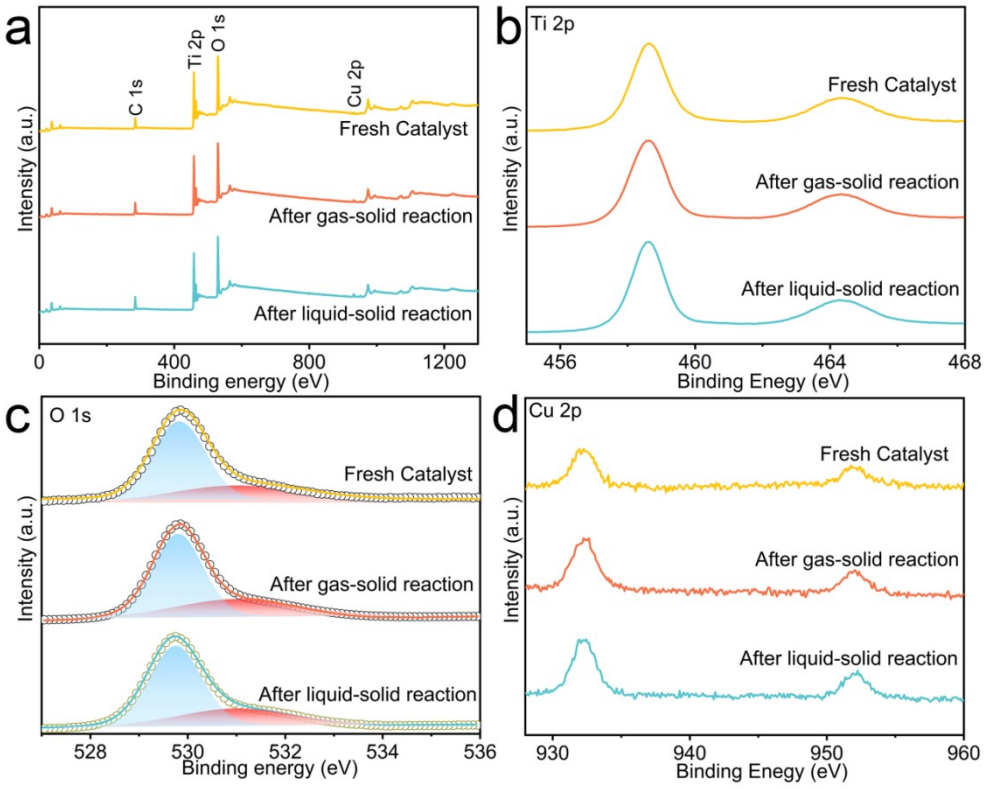

Fig. S8. (a) XPS survey, (b) Ti 2p, (c) O 1s, (d) Cu 2p XPS spectra of $Cu_{0.01}$/3DOM-TiO_2 before and after cyclic reactions.

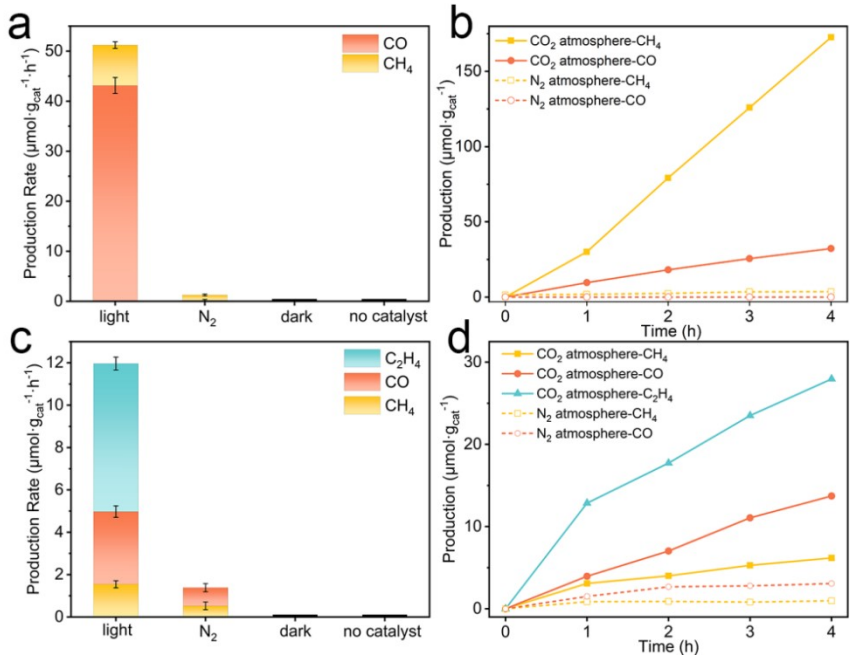

Fig. S9. (a) Product formation rates under different conditions and (b) time-dependent product yields in CO_2 and N_2 atmosphere for gas-solid catalytic system. (c) Product formation rates under different conditions and (d) time-dependent product yields in CO_2 and N_2 atmosphere for liquid-solid catalytic system.

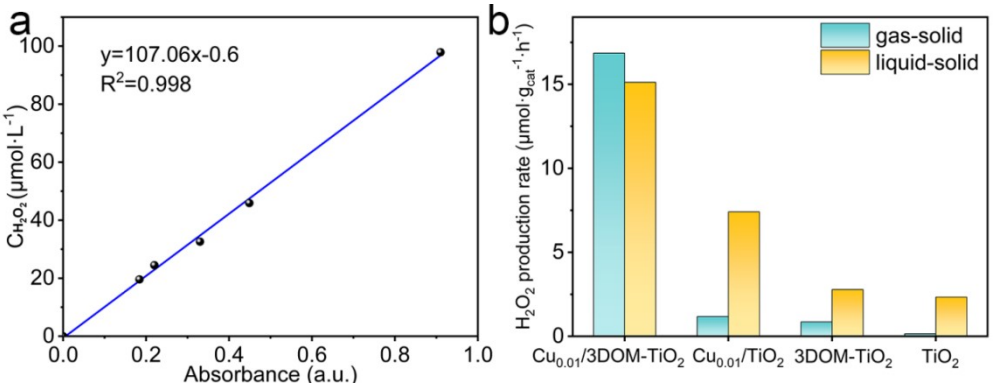

Fig. S10. (a) Standard calibration curve for the quantitation of hydrogen peroxide. (b) H_2O_2 production rates over different photocatalysts in both reaction systems.

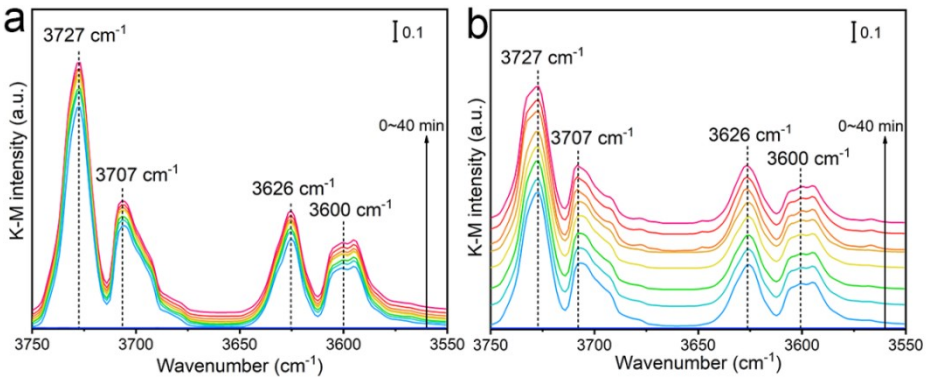

Fig. S11. *In situ* DRIFTS spectra in the region of 3550 ~ 3750 cm^{-1} of the photocatalytic CO_2 reduction with $Cu_{0.01}$/3DOM-TiO_2 catalyst in two different systems: (a) liquid-solid catalytic system, (b) gas-solid catalytic system.

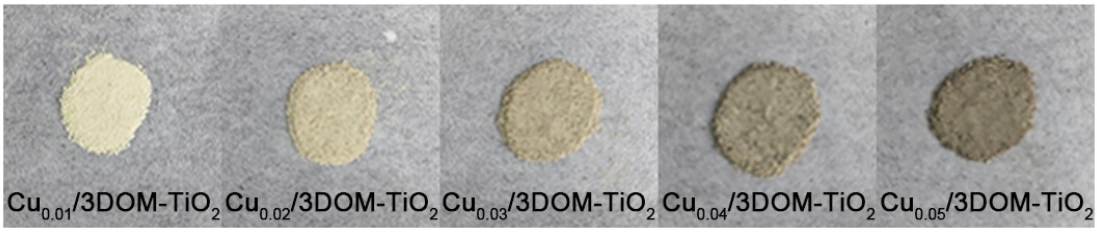

Fig. S12. Digital images of Cu_x/3DOM-TiO_2 photocatalysts with different Cu contents.

3. Supplementary Tables

Table S1. Anatase and rutile TiO_2 contents of several different photocatalysts.

Entry	Sample	Anatase TiO_2 (wt%)	Rutile TiO_2 (wt%)*
1	$Cu_{0.01}$/3DOM-TiO_2	86.14	13.86
2	$Cu_{0.01}$/TiO_2	100	0
3	3DOM-TiO_2	86.20	13.80
4	TiO_2	100	0

*The mass fractions of rutile TiO_2 (W_{Rutile}) are calculated according to the formula $W_{Rutile} = A_{Rutile}/(0.884\ A_{Anatase} + A_{Rutile})$,[S1-S2] where $A_{Anatase}$ and A_{Rutile} are the integrated intensities of anatase (101) and rutile (110) XRD peaks, respectively.

Table S2. BET surface areas, pore volumes and average pore sizes of $Cu_{0.01}$/3DOM-TiO_2, 3DOM-TiO_2 and $Cu_{0.01}$/TiO_2 samples.

Photocatalyst	BET surface area (m^2/g)	Pore volume (cm^3/g)	Average pore size (nm)
$Cu_{0.01}$/3DOM-TiO_2	52.80	0.28	18.59
3DOM-TiO_2	48.97	0.22	17.44
$Cu_{0.01}$/TiO_2	3.74	0.0014	50.69

Table S3. Product formation rates of photocatalytic CO_2 reduction with different

photocatalysts in liquid-solid catalytic system. Reaction conditions: 5 mg photocatalyst, 30 mL H_2O, CO_2 atmosphere, Xe lamp with optical power density of 200 mW·cm^2, 4 h irradiation.

Entry	Photocatalyst	CH_4 ($\mu mol \cdot g_{cat}^{-1} \cdot h^{-1}$)	CO ($\mu mol \cdot g_{cat}^{-1} \cdot h^{-1}$)	C_2H_4 ($\mu mol \cdot g_{cat}^{-1} \cdot h^{1}$)
1	$Cu_{0.01}$/3DOM-TiO_2	1.54	3.43	6.99
2	$Cu_{0.01}$/TiO_2	0	0.78	0
3	3DOM-TiO_2	0	1.91	0
4	TiO_2	0	0.41	0

Table S4. Product formation rates of photocatalytic CO_2 reduction with different photocatalysts in gas-solid catalytic system. Reaction conditions: 5 mg photocatalyst, 1 mL H_2O for providing water vapor, CO_2 atmosphere, Xe lamp with optical power density of 200 mW·cm^2, 4 h irradiation.

Entry	Photocatalyst	CH_4 ($\mu mol \cdot g_{cat}^{-1} \cdot h^{-1}$)	CO ($\mu mol \cdot g_{cat}^{-1} \cdot h^{-1}$)
1	$Cu_{0.01}$/3DOM-TiO_2	43.15	8.06
2	$Cu_{0.01}$/TiO_2	0	2.02
3	3DOM-TiO_2	0	2.80
4	TiO_2	0	1.10

Table S5. Product formation rates from the cyclic experiments of the photocatalytic

CO_2 reduction with $Cu_{0.01}$/3DOM-TiO_2 catalyst in liquid-solid catalytic system. Reaction conditions: 5 mg photocatalyst, 30 mL H_2O, CO_2 atmosphere, Xe lamp with optical power density of 200 mW·cm^2, 4 h for each cycle.

Cycle	CH_4 ($\mu mol \cdot g_{cat}^{-1} \cdot h^{-1}$)	CO ($\mu mol \cdot g_{cat}^{-1} \cdot h^{-1}$)	C_2H_4 ($\mu mol \cdot g_{cat}^{-1} \cdot h^{1}$)
1	1.54	3.43	6.99
2	1.41	3.37	6.85
3	1.38	3.18	6.49
4	1.32	3.08	6.15

Table S6. Product formation rates from the cyclic experiments of the photocatalytic CO_2 reduction with $Cu_{0.01}$/3DOM-TiO_2 catalyst in gas-solid catalytic system. Reaction conditions: 5 mg photocatalyst, 1 mL H_2O for providing water vapor, CO_2 atmosphere, Xe lamp with optical power density of 200 mW·cm^2, 4 h for each cycle.

Cycle times	CH_4 ($\mu mol \cdot g_{cat}^{-1} \cdot h^{-1}$)	CO ($\mu mol \cdot g_{cat}^{-1} \cdot h^{-1}$)
1	43.15	8.06
2	42.85	7.46
3	42.64	7.21
4	39.22	6.80

Table S7. H_2O_2 production rates in the photocatalytic CO_2 reduction reaction systems

with different photocatalysts.

Entry	Photocatalyst	H_2O_2 production rate in gas-solid system ($\mu mol \cdot g_{cat}^{-1} \cdot h^{-1}$)	H_2O_2 production rate in gas-solid system ($\mu mol \cdot g_{cat}^{-1} \cdot h^{-1}$)
1	$Cu_{0.01}$/3DOM-TiO_2	16.85	15.12
2	$Cu_{0.01}$/TiO_2	1.18	7.41
3	3DOM-TiO_2	0.86	2.78
4	TiO_2	0.15	2.34

Table S8. Comparison between the catalytic activities of $Cu_{0.01}$/3DOM-TiO_2 and the previously reported 3DOM-TiO_2 based photocatalysts for CO_2 reduction.

Entry	Catalyst	Reactant	Light	Products ($\mu mol \cdot g_{cat}^{-1} \cdot h^{-1}$)	Ref. No.
1	$Cu_{0.01}$/3DOM-TiO_2	CO_2 + H_2O vapor	300 W Xe lamp (200 mW/cm^2)	CH_4, 43.15 CO, 8.06	This work
2	$Cu_{0.01}$/3DOM-TiO_2	CO_2 + 30 mL H_2O	300 W Xe lamp (200 mW/cm^2)	CH_4, 1.54 CO, 3.43 C_2H_4, 6.99	This work
3	3DOM Au_8/TiO_2	CO_2 + H_2O vapor	300 W Xe lamp with a 420 nm UV-cutoff filter	CH_4, 2.88	S3
4	3DOM Pt@CdS/TiO_2	CO_2 + H_2O vapor	300 W Xe lamp (100 mW/cm^2)	CH_4, 36.8 CO, 0.7 H_2, 16.2	S4
5	AuPd/3DOM-TiO_2	CO_2 + 2 mL H_2O	300 W Xe lamp (80 mW/cm^2)	CH_4, 18.5 CO, 1.2 H_2, 18.6	S5
6	Pt/3DOM TiO_2-SiO_2	CO_2 + 1 mL H_2O	300 W Xe lamp with an AM 1.5 filter	CH_4, 9.7 CO, 1.8 H_2, 58.7	S6
7	Au/RuO_2/3DOM TiO_2-SiO_2	CO_2 + 1 mL H_2O	300 W Xe lamp with an AM 1.5 filter	CH_4, 5.7 CO, 1.2 H_2, 2.5	S7
8	g-C_3N_4/Pt/3DOM-TiO_2@C	CO_2 + 2.5 mL H_2O	300 W Xe lamp with a 420 nm UV-cutoff filter	CH_4, 6.56 CO, 1.47 H_2, 0.82	S8
9	MoS_2/3DOM-TiO_2	CO_2 + 2.5 mL H_2O	300 W Xe lamp	CH_4, 2.83 CO, 1.47	S9

References

S1 Q. Xu, Y. Ma, J. Zhang, X. Wang, Z. Feng and C. Li, Enhancing hydrogen production activity and suppressing CO formation from photocatalytic biomass reforming on Pt/TiO_2 by optimizing anatase–rutile phase structure, *J. Catal.*, 2011, **278**, 329-335.

S2 X. Wang, S. Shen, Z. Feng and C. Li, Time-resolved photoluminescence of anatase/rutile TiO_2 phase junction revealing charge separation dynamics, *Chin. J. Catal.*, 2016, **37**, 2059-2068.

S3 J. Jiao, Y. Wei, Z. Zhao, W. Zhong, J. Liu, J. Li, A. Duan and G. Jiang, Synthesis of 3D ordered macroporous TiO_2-supported Au nanoparticle photocatalysts and their photocatalytic performances for the reduction of CO_2 to methane, *Catal. Today* 2015, **258**, 319-326.

S4 Y. Wei, J. Jiao, Z. Zhao, W. Zhong, J. Li, J. Liu, G. Jiang and A. Duan, 3D ordered macroporous TiO_2-supported Pt@CdS core–shell nanoparticles: design, synthesis and efficient photocatalytic conversion of CO_2 with water to methane, *J. Mater. Chem. A*, 2015, **3**, 11074-11085.

S5 J. Jiao, Y. Wei, Y. Zhao, Z. Zhao, A. Duan, J. Liu, Y. Pang, J. Li, G. Jiang and Y. Wang, AuPd/3DOM-TiO_2 catalysts for photocatalytic reduction of CO_2: High efficient separation of photogenerated charge carriers, *Appl. Catal., B*, 2017, **209**, 228-239.

S6 C. Dong, C. Lian, S. Hu, Z. Deng, J. Gong, M. Li, H. Liu, M. Xing and J. Zhang, Size-dependent activity and selectivity of carbon dioxide photocatalytic reduction over platinum nanoparticles, *Nat. Commun.*, 2018, **9**, 1252.

S7 C. Dong, S. Hu, M. Xing and J. Zhang, Enhanced photocatalytic CO_2 reduction to CH_4 over separated dual co-catalysts Au and RuO_2, *Nanotechnology*, 2018, **29**, 154005.

S8 C. Wang, X. Liu, W. He, Y. Zhao, Y. Wei, J. Xiong, J. Liu, J. Li, W. Song, X. Zhang and Z. Zhao, All-solid-state Z-scheme photocatalysts of g-C_3N_4/Pt/macroporous-(TiO_2@carbon) for selective boosting visible-light-driven conversion of CO_2 to CH_4, *J. Catal.*, 2020, **389**, 440-449.

S9 Y. Li, J. Tang, Y. Wei, W. He, Z. Tang, X. Zhang, J. Xiong and Z. Zhao, The heterojunction between 3D ordered macroporous TiO_2 and MoS_2 nanosheets for enhancing visible-light driven CO_2 reduction, *J. CO_2 Util.*, 2021, **51**, 101648.